

Insights into the structure of the LC13 TCR/HLA-B8-EBV peptide complex with molecular dynamics simulations

Athanassios Stavrakoudis

Published online: 21 January 2011
© Springer Science+Business Media, LLC 2011

Abstract One key step in the immune response against infected or tumor cells is the recognition of the T-cell receptor (TCR) by class I major histocompatibility complexes. The complex between the HLA-B8 molecule and the immunodominant peptide with sequence FLRGRAYGL, derived from the *Epstein-Barr virus*, with the LC13 TCR has been determined by X-ray diffraction. The complex has been used as a starting point in a molecular dynamics study in order to investigate the dynamics of the complex association and to explore the specific interactions of the complex formation. The analyzed structures provided evidence that the peptide adopts an open type β -turn conformation close to C-terminal part, which dominates peptide/TCR interactions. Conformational energy landscape analysis indicated the presence of two conformational clusters in the peptide's structure, underlying the backbone flexibility of the peptide despite being surrounded by two receptors. The peptide/MHC/TCR interface was found to hold significant number of solvent molecules, more specifically the peptide has been found to have approximately seventeen hydrogen bonds with water molecules. The molecular dynamics simulation indicated the disruption of some MHC/TCR contacts, mainly with the CDR1 α loop. However, several other interactions emerged that resulted in a stable association during the 20 ns trajectory, as revealed by the buried surface area analysis.

Keywords β -turn · *Epstein-Barr virus* · HLA-B8 · Molecular dynamics · pMHC/TCR interactions · TCR interactions

Introduction

The recognition of antigenic peptides (p) bound to major histocompatibility complex (MHC) by the T-cell antigen receptors (TCR) is the basis of adaptive immune response. The biomolecular association of pMHC and TCR triggers the cytotoxic T lymphocyte activation and results in targeting cell destruction [1]. The molecular interactions that take place at the pMHC/TCR binding interface is of great interest. Three dimensional structure of pMHC, TCR, and pMHC/TCR complexes, provide a unique insight in atomistic detailed manner of their structure and interactions [2, 3]. Recognition of pMHC complexes by TCRs follows complex thermodynamics without a clear “signature” [4, 5]. It is not clear how pMHC/TCR binding leads to T-cell activation. However, several researchers have proposed the correlation of this binding process with the dissociation rate constant [6], or the serial triggering, thus with the number of events that occur sequentially in the binding process [7], or with the change in heat capacity [8].

The structure and conformation of a peptide in the MHC's binding groove affects significantly the recognition of pMHC complex by the TCR [9, 10]. Thus, a closer look to peptide's and receptor's conformational features, would be likely of benefit in our effort to understand the mechanism of pMHC/TCR recognition. Computer simulation of molecular dynamics is a well-established method for studying several aspects of biomolecular structure and function [11–13]. Moreover, biomolecular modeling can complement experimental studies [14–16] and recent

A. Stavrakoudis (✉)
Department of Economics, University of Ioannina,
451 10 Ioannina, Greece
e-mail: astavrak@cc.uoi.gr
URL: <http://stavrakoudis.econ.uoi.gr>

studies have been used in order to elucidate dynamics of immunological complexes [17–22], in epitope prediction [23], or even more excitingly in patient decision strategies [24]. Despite the huge progress in parallel computation during last years, simulation of immunological synapse is far from being a trivial procedure [22]. However, it offers a well-tested background for atomistic view in such binding processes [18, 25]. In addition, many researchers have applied molecular dynamics simulations to investigate the energetics of pMHC/TRC complex association [26–28].

In this study, the dynamics of the T-cell receptor LC13 in complex with HLA-B*0801/FLRGRAYGL has been investigated with molecular dynamics simulation. The published structure [29] solved by X-ray diffraction, served as an initial point to set up this study. The results confirmed the suggested high mobility of the TCR's loops (complementary determining regions, CDRs) that interact with pMHC complex. Moreover, special attention has been drawn on the peptide's structure. Under the light of the current investigation, it is proposed that the Arg₅–Gly₈ fragment of the peptide, which is responsible for the peptide/TCR contacts adopts an open type β -turn conformation [30]. Despite the many hydrophobic interactions between the pMHC complex and the CDR3 β loop of the TCR, it has been found that the polar groups at the protein/protein interface remained highly hydrated, underlying the role of the water in the complex association and stability.

Methods

Initial coordinates of the complex were downloaded from Protein Data Bank [31] access code: 1mi5 [29]. Hydrogen atoms were added with the VMD program [32] and its autopsf utility. Topology and force field parameters for all atoms were assigned from the CHARMM27 parameter set [33]. Protonation status of Histidine side chains was determined with the REDUCE program [34]. The TCR/pMHC complex was centered in a rectangular box with dimensions $101.4 \times 90.5 \times 174.7 \text{ \AA}^3$. The box was filled with TIP3P water molecules [35]. Adequate distance between the solute and the edge of the simulation box is needed in order to minimize artifacts [36], thus the box dimensions were chosen so that any protein atom had a distance of at least 17 \AA with box edges. Crystallographic water molecules (282) were included in the model. The final system contained 45,369 water molecules. The system was electrostatically neutralized by with the addition of 53 Na⁺ and 31 Cl⁻ ions, respectively, to mimic a salt concentration on 0.1 mM. Total number of atoms of the whole system was 149,121.

Non-bonded van der Waals interactions were gradually turned off at a distance between 12 and 14 \AA . Long range

electrostatics were calculated with the PME method [37]. Non-bonded forces and PME electrostatics were computed every second step. Pair list was updated every 10 steps. Bonds to hydrogen atoms were contained with the SHAKE method [38] allowing a 2 fs time step for the integration. The system was initially subjected to energy minimization with 25,000 steps. The temperature of the system was then gradually increased to 310 K, with Langevin dynamics using the NVT ensemble, during a period of 30,000 steps, by stepwise reassignment of velocities every 5,000 steps. The simulation was continued at 310 K for 100,000 steps (200 ps). During minimization and equilibration phases, protein backbone atoms (N, C $^{\alpha}$, C', O) and oxygen atoms of crystallographic waters were restrained to their initial positions with a force constant of $50 \text{ kcalmol}^{-1} \text{ \AA}^{-2}$. The system was equilibrated for another 200 ps with the force constant reduced to $5 \text{ kcalmol}^{-1} \text{ \AA}^{-2}$. Finally, 400 ps of NVT simulation at 310 K were performed with total elimination of the positional restraints. The simulation was passed to the productive phase, by applying constant pressure with the Langevin piston method [39]. Pressure was maintained at 1 atm and temperature at 310 K. Results are based to a period of 20 ns of this isothermal-isobaric (NPT) run. Snapshots were saved to disk at 1 ps interval for structural analysis.

Trajectory analysis was performed with the Eucb [40] software package. In cases of angle/dihedral statistics, the Yamartino method has been applied in order to get mean and standard deviation values [41, 42], as implemented with the Eucb software [40]. For the calculation of hydrogen bond interaction a single geometrical criterion was applied: a hydrogen bond existed if the donor–acceptor was less than 3.3 \AA and their donor–hydrogen–acceptor angle was bigger than 120° . Hydrophobic interactions with residues with aliphatic or aromatic side chains were also calculated on a distance basis: two side chains were considered to make hydrophobic contacts if the minimum distance between any two carbon side chain atoms were in proximity of less than 4 \AA . A sequence of four residues was considered to form a β -turn if the C $_i^{\alpha}$ –C $_{i+3}^{\alpha}$ distance was less than 7 \AA and the C $_i^{\alpha}$ –C $_{i+1}^{\alpha}$ –C $_{i+2}^{\alpha}$ –C $_{i+3}^{\alpha}$ dihedral angle was bigger than 90° [43, 44]. As recently has been proposed, an open type turn might be accepted with C $_i^{\alpha}$ –C $_{i+3}^{\alpha}$ distances up to 10 \AA [30]. Structural figures were prepared with PyMOL (www.pymol.org).

Correlated motions have been estimated from the normalized covariance (correlation) matrix of C $^{\alpha}$ distances. The matrix's elements are the correlations in motion of the residues. Values are (ideally) equal to 1 if two residues move in the same direction or (ideally) equal to -1 if they move in opposite directions, and are equal to 0 if their motion is uncorrelated. However, in practice, the values are

spread in the $[-1,1]$ range. The software package Carma [45] has been used to obtain the normalized covariance matrix and for principal component analysis.

Calculation of buried surface area (BSA) was performed with the NACCESS program [46], based on the formula:

$$BSA = S_p + S_t - S_c \quad (1)$$

thus as the difference of the surface accessible area of the complex (S_c) from the sum of the of surface accessible areas of the pMHC (S_p) and TCR molecules (S_t), respectively.

Entropy was estimated with quasi harmonic analysis based on Schlitter's [47] and Andricioaei [48] methods.

To facilitate the comparison between the PDB initial structure and the MD trajectory frames, the naming scheme of the polypeptide chains was adapted from the PDB file. Thus, chain A represents the α of the MHC molecule, chain B represents the β (microglobulin) of the MHC molecule, chain C represents the peptide, chain D represents the α chain of the T-cell receptor and chain E represents the β chain of the T-cell receptor. In this scheme, residue Leu_{2C} is the second residue of the peptide sequence and residue Leu_{94D} is the Leu-94 residue from the TCR's α chain.

Results

Stability of the Trajectory

The simulation of the pMHC/TCR complex resulted in a quite stable trajectory, without major conformational transitions. The radius of gyration of the complex increased from 38.2 Å (X-ray initial structure) to approximately 39.3 Å during the first 3 ns of the simulation. It fluctuated between 38.2 and 39.5 Å and averaged at 38.9(0.2) Å for the rest of the trajectory. The same impression can be extrapolated from the root mean square fluctuation (RMSF) of C $^{\alpha}$ atoms and time evolution of root mean square deviation (RMSD) of backbone atoms as they are illustrated in Fig. 1. The α_1 and α_2 helices of the MHC remained also stable, although some concern has been published about the disruption of helical structures in small helical peptides [49, 50]. A movie assembled from 200 snapshots of the MD trajectory (one every 100 ps), can be found as supplementary material from the website of the publisher, as a visual demonstration of the dynamics of the pMHC/TCR complex.

Backbone Dynamics of the Peptide

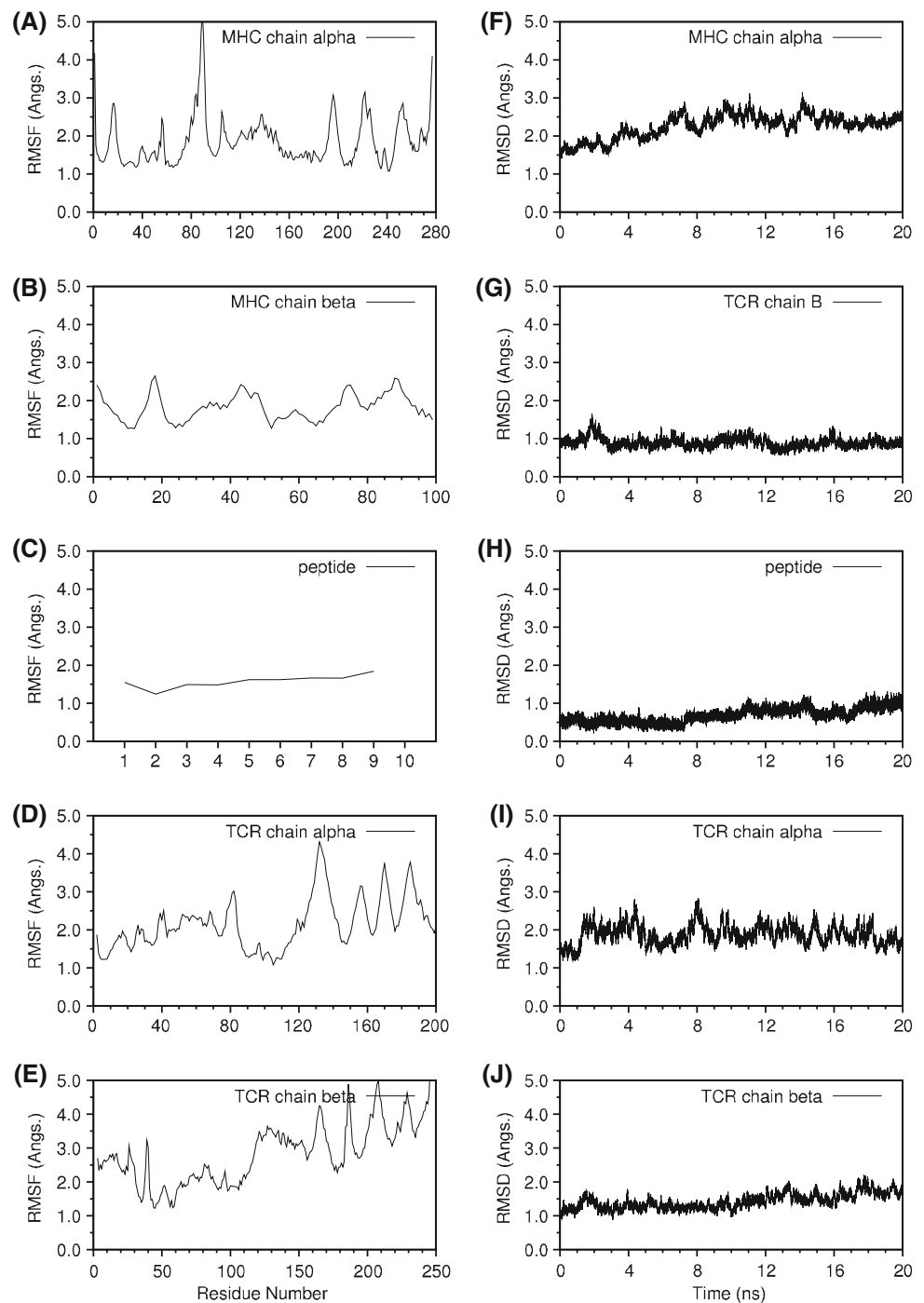
As it can be seen from Fig. 1, the FLRGRAYGL peptide showed minimal RMSF and RMSD values, for C $^{\alpha}$ and backbone atoms, respectively. Similarly, time evolution of backbone dihedral angles remained very close to the initial

values, without any major transition. The RMSD values of the backbone atoms of chain C (peptide) varied between 0.2 and 1.3 Å with average value of 0.68(0.19). These values are considered rather small and are indicative of stable structures during MD trajectories. Figure 2 shows the initial X-ray structure of the peptide along with some snapshots taken from the MD trajectory and demonstrates the similarity between X-ray and simulated peptide structures.

To further assess this point, the conformational energy landscape of the peptide has been constructed. It has been recently argued that dihedral angle principal component analysis should be used, in place of Cartesian PCA in order to correctly locate the energy minima [51]. Both methods have been used, in order to compare their results, which are shown in Fig. 3. Both methods indicate that the peptide's conformation can be clustered in two main clusters. The separation is more clearly seen in the dihedral PCA plots (bottom row of Fig. 3). This analysis also suggests the partial coverage of the conformational space covered through the 20 ns MD simulation and the incomplete convergence of the trajectory. The fact that RMS analysis can not fully uncover the dynamics of biomolecular association and that PCA is needed in order to discriminate the possible clusters observed through MD trajectories has been recently pointed out [52]. Fig. 4 demonstrates the difference in backbone conformation in the two main clusters. As it can be seen, there is only a 1.5 Å displacement of the Gly_{8C}:C $^{\alpha}$ atom that basically discriminates the two conformers. Such small movements of the peptide's atoms in the MHC binding groove can affect drastically binding affinity or pMHC complexes [53].

The structure of the peptides into the MHC's binding groove is (in general) in extended conformation, bulged in the central part of the sequence which is exposed to TCR interface. Given the fact that the peptide is surrounded by receptor residues from all directions, the MHC's β floor and α_1, α_2 helices and TCR's CDRs, it is quite surprising that there was space for conformational "maneuvers". Thus, as the PCA was indicative for such a situation, the peptide was subjected to secondary structure analysis. Analysis of the initial conformation with the program STRIDE [54] indicated an extended conformation with all backbone ϕ angles to have negative values ranged from -45° to -123° , and all backbone ψ angles to have positive values ranged from 110° to 160° . The only exception was the Ala_{6C}'s ψ value which was found -25° . This exception at position P5 or P6 is quite common in pMHC complexes, and it is responsible for the "bulged" conformation in the central part of the peptide. The results from the secondary structure analysis revealed an interesting feature, as the peptide was found to form a β -turn in the 5–8 region for approximately 59% of the trajectory frames. However, it must be noted that a revised set of descriptors for classification of β -turns has been recently

Fig. 1 Root mean square fluctuation (RMSF) of C^α atoms during the MD trajectory, and root mean square deviation (RMSD) time series of backbone atoms (N, C^α , C) of the pMHC/TCR complex after fitting the corresponding atom positions from MD trajectory to initial (X-ray) coordinates. **a** RMSF of C^α atoms of the MHC chain α , **b** RMSF of C^α atoms of MHC chain β , **c** RMSF of C^α atoms of the peptide, **d** RMSF of C^α atoms of TCR chain α , **e** RMSF of C^α atoms of TCR chain β , **f** RMSD of backbone atoms of MHC chain α , **g** RMSD of backbone atoms of MHC chain β , **h** RMSD of backbone atoms of the peptide, **i** RMSD of backbone atoms of TCR chain α , **j** RMSD of backbone atoms of TCR chain β



proposed [30], and an open type β -turn, without a hydrogen bond, can have a distance up to 10 Å. If we take into consideration that the maximum $\text{Arg}_{5C}:C^\alpha\text{--Gly}_{8C}:C^\alpha$ distance was 7.9 Å, and the maximum $\text{Arg}_{5C}:C^\alpha\text{--Ala}_{6C}:C^\alpha\text{--Tyr}_{7C}:C^\alpha\text{--Gly}_{8C}:C^\alpha$ dihedral angle was 59° , then it can be considered that the $\text{Arg}_{5C}\text{--Gly}_{8C}$ fragment remained in stable β -turn conformation for the whole trajectory. The β -turn was not characterized by a stabilizing hydrogen bond. If this was a well-characterized normal β -turn, then it

would be expected that a hydrogen bond would exist between $\text{Arg}_{5C}:O$ and $\text{Gly}_{8C}:N$ atoms. However, detection of peptide's hydrogen bonds revealed the $\text{Arg}_{5C}:O$ was hydrogen bonded with MHC's $\text{Thr}_{73A}:O^{\gamma 1}$ atom (Table 2). Classification based on backbone dihedral angles revealed that the turn can be of type VIa or IV.

Turn-like structures have been observed in other pMHC and pMHC/TCR complexes as well. For example, the decamer peptide KAFSPEVIPMF has been found to form a

Fig. 2 Backbone alignment of the peptide's X-ray structure (carbon atoms in *magenta*) with representative frames of the MD trajectory (carbon atoms in *green*). Snapshots were taken at 4, 8, 12, 16, and 20 ns. For the interpretation of colors in this figure, the reader is referenced to the web version of this article (Color figure online)

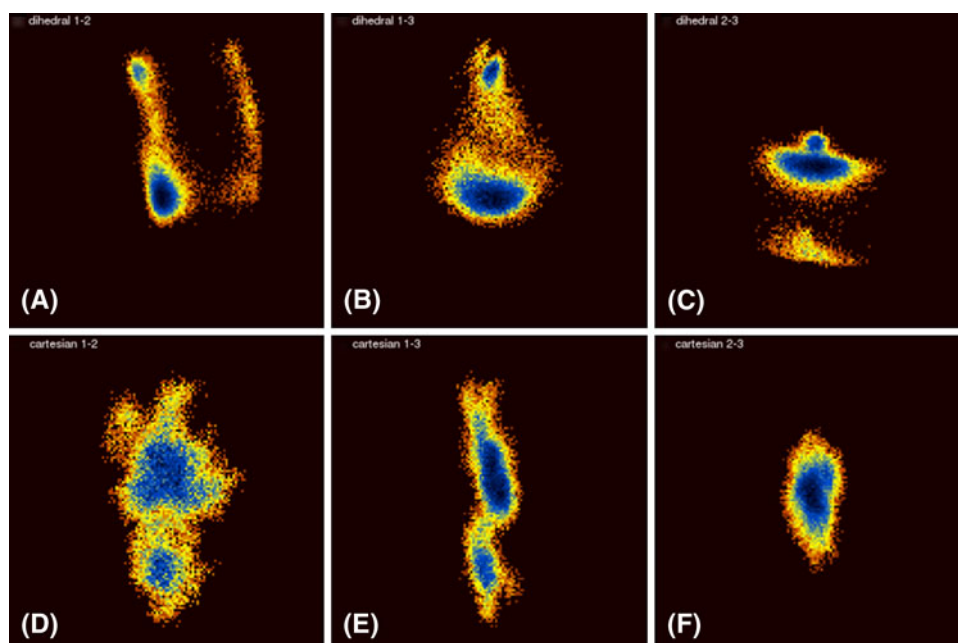
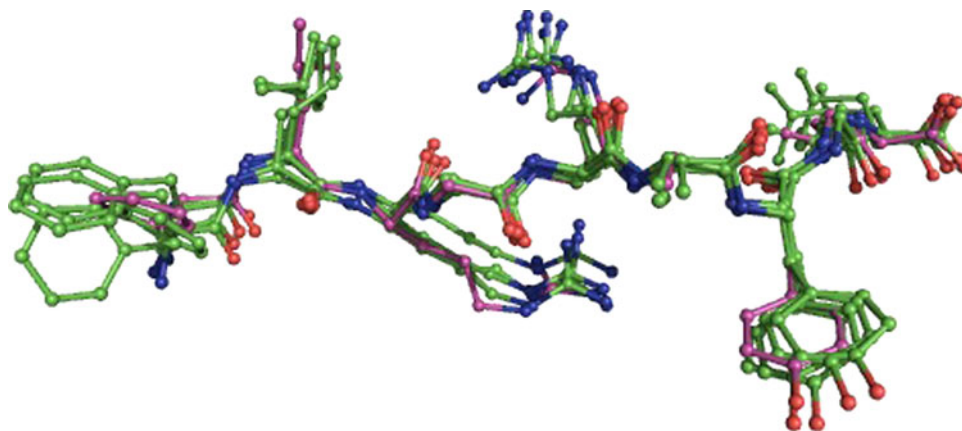


Fig. 3 Cartesian (top row) and dihedral (bottom row) principal component analysis of the peptide's backbone atoms. The diagram is a pseudo-color representation of the density function corresponding to the projections of the fluctuation of the motion on the planes of the top two eigenvectors. The density function shown is $\Delta G = -k_B \ln(p/p_{\max})$ where k_B is the Boltzmann constant, T is the temperature in Kelvin, and p and p_{\max} are probabilities obtained from the distribution of the principal components for each structure (frame) from the molecular dynamics trajectory. The raw data were binned on a square

type VIII β -turn in the region Pro₅-Ile₈ when bound to the HLA-B*5703 MHC class I molecule [55] (PDB code: 2bvo). Also the peptide EENLLDFVRF was found in type II β -turn when bound to HLA-B*4405 MHC class I molecule or in type IV β -turn when the pMHC complex associated with the DM1 T-cell receptor [56] (PDB codes 3dx8 and 3dxa, respectively). However, it must be noted that type IV or VIII β -turns are not characterized by a hydrogen bond interaction [43]. Sometimes, the existence of β -turn peptides in immunological complexes have been

underestimated [57]. Here, a comprehensive look at this particular feature of peptide's structure is attempted. Characterization of the β -turn observed in the Arg_{5C}-Gly_{8C} region of the FLRGRAYGL peptide is demonstrated in Fig. 5.

In order to see if there was any time trend in the formation of the β -turn, the 20 ns MD trajectory was split in ten fragments of 2 ns each and the occurrence of β -turn was measured in each fragment. Results of this procedure are shown at Table 1. As it can be seen, there is no specific

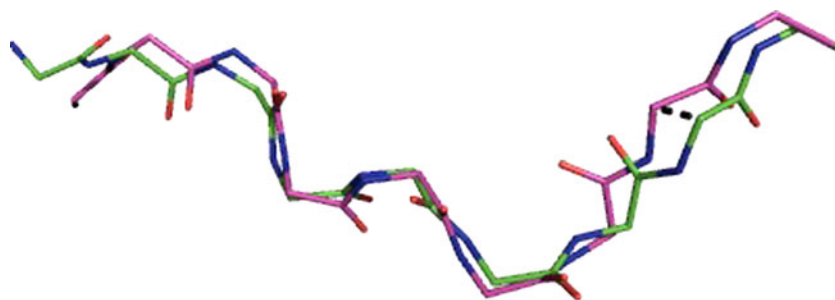


Fig. 4 Backbone structure of the FLRGRAYGL peptide. Two conformations are depicted (at 5 and 20 ns) of the MD trajectory to demonstrate the subtle difference around the Arg_{5C}–Gly_{8C} region. A small displacement of only 1.5 Å at the Gly_{8C}:C^α atom between the

two conformers (dashed line) determines the conformational clusters identified by PCA analysis: with (colored with magenta) or without (colored with green) β-turn (Color figure online)

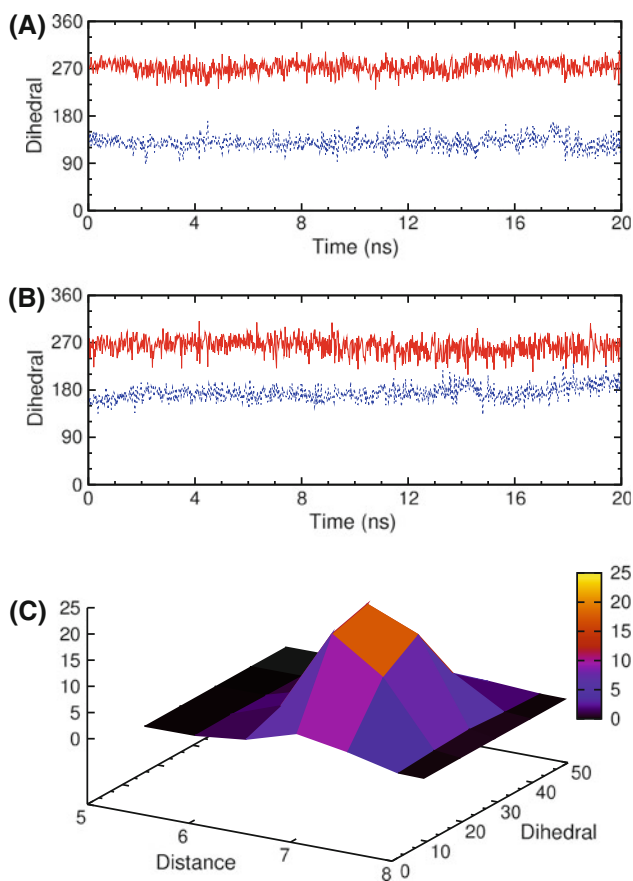


Fig. 5 Characterization of the possible β-turn around the Arg_{5C}–Gly_{8C} peptide sequence. Dihedral angles ϕ and ψ are plotted with red and blue color, respectively and have been converted in the [0,360] range to facilitate the time series plots. **a** Time evolution of ϕ , ψ dihedral angles of the residue Tyr₇. **b** Time evolution of ϕ , ψ dihedral angles of the residue Gly₈. **c** 3D plot of the probability of the distance (in Å) Arg_{5C}:C^α–Gly_{8C}:C^α and the dihedral angle Arg_{5C}:C^α–Ala_{6C}:C^α–Tyr_{7C}:C^α–Gly_{8C}:C^α. The probability is shown in the z-axis as percentage of frames. For the interpretation of colors in this figure, the reader is referenced to the web version of this article (Color figure online)

time trend in the β-turn formation. The β-turn is the dominant conformation in the first two parts. Then, for approximately 8 ns, the β-turn conformation is met to less

Table 1 Count of β-turn occurrence of the peptide’s secondary structure, in the Arg_{5C}–Gly_{8C} region, for different time frames of the MD trajectory

Frame1	Frame2	No of frames		
		Total	Type VIb	Type IV
1	2000	1655	956	699
2001	4000	1714	922	792
4001	6000	943	471	472
6001	8000	781	356	425
8001	10000	815	376	439
10001	12000	932	430	502
12001	14000	1068	470	598
14001	16000	1368	622	746
16001	18000	1345	639	706
18001	20000	1223	573	650

than the half of the trajectory frames. During the last 8 ns it becomes again the dominant conformation. During the whole trajectory, 6,452 events of turn breaking/formation have been found. On average, this means that every 3 ps the conformation changed status.

One interesting thing is the fluctuation observed in C^α–C^α distances of residues Phe_{1C} and Leu_{9C}, thus the N- and C-terminals of the peptide. In order to explore the correlation of residue movements of the peptide, the normalized covariance matrix of the C^α atoms has been computed. All values were positive and ranged from 0.56 (Phe_{1C}–Leu_{9C}) to 0.97 (Arg_{5C}–Ala_{6C}), indicating a highly positive correlation of atom motions. One thing that can be easily extracted from the part D) of Fig. 6 (scatter plot of distances Phe_{1C}:C^α–Leu_{9C}:C^α and Arg_{5C}:C^α–Leu_{9C}:C^α) is that there is a correlation between these two distances. The correlation coefficient of these two quantities is 0.66. One prerequisite for the formation of a β-turn is the approximation of the C^α of residues at position $i, i + 3$ to a distance less than 7 Å. Thus, it could be expected that frames with this conformation will have a more “folded” peptide

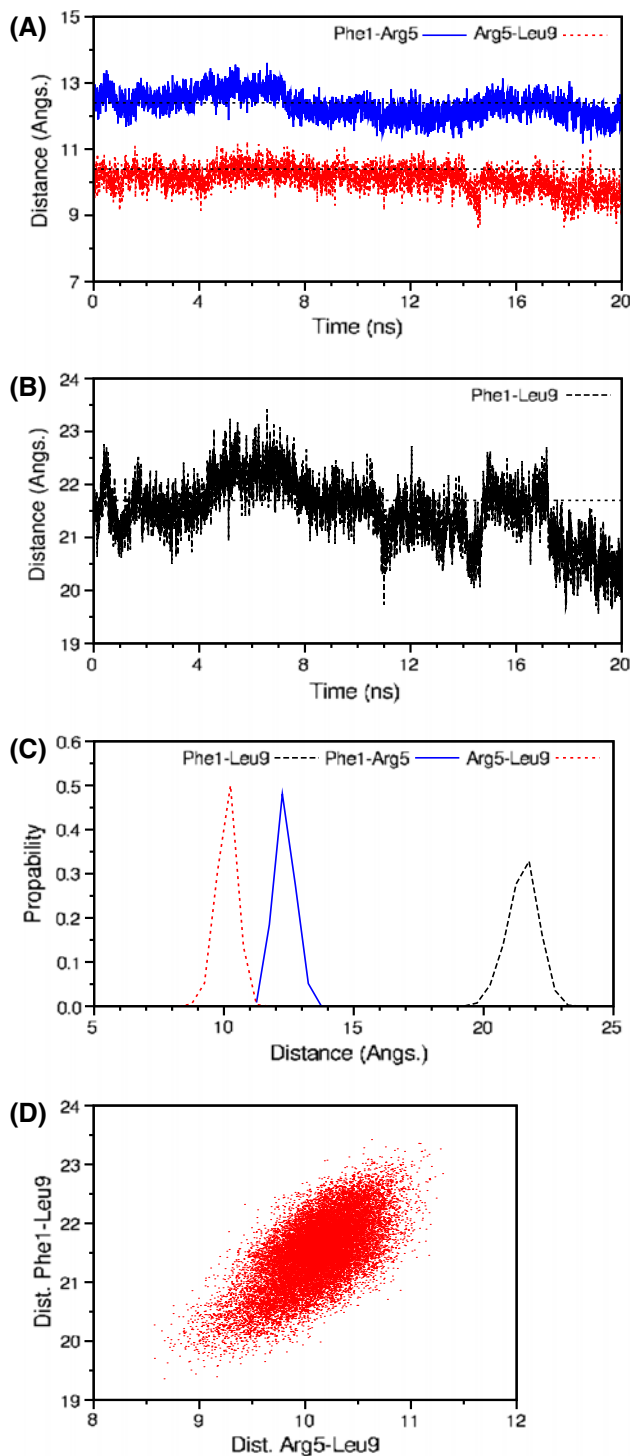


Fig. 6 **a** Time evolution of Phe_{1C}:C^α-Arg_{5C}:C^α and Arg_{5C}:C^α-Leu_{9C}:C^α distances. Horizontal lines at 12.4 and 10.4 Å indicate the corresponding distances in the X-ray structure. **b** Time evolution of Phe_{1C}:C^α-Leu_{9C}:C^α distance. Horizontal line at 21.7 Å indicates the corresponding distance in the X-ray structure. **c** Histogram of distance distribution between Phe_{1C}:C^α-Leu_{9C}:C^α, Phe_{1C}:C^α-Arg_{5C}:C^α and Arg_{5C}:C^α-Leu_{9C}:C^α pairs. **d** Scatter plot of Phe_{1C}:C^α-Arg_{5C}:C^α and Arg_{5C}:C^α-Leu_{9C}:C^α distances. For the interpretation of colors in this figure, the reader is referred to the web version of this article

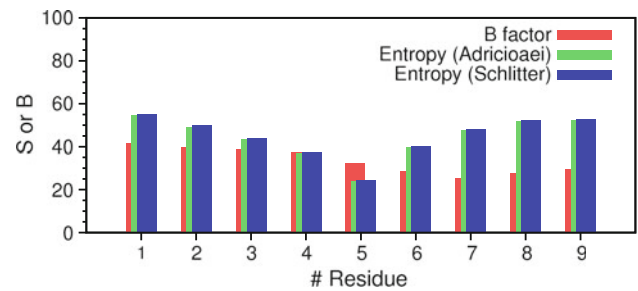


Fig. 7 Comparison of B factor (B) of peptide's C^α atoms with entropy (S) of the backbone atoms. B factor values were taken from the PDB file (1mi5). Entropy per residue for backbone atoms was calculated with both Schlitter and Andriociaei approximations (see "Methods" for details). Entropy's (S) units is J/mol/K. For the interpretation of colors in this figure, the reader is referred to the web version of this article

backbone with shortened Phe_{1C}:C^α-Leu_{9C}:C^α distance. Indeed, as indicated from the MD analysis, this is exactly the case.

From the analysis of Fig. 6, it can be concluded that the Phe_{1C}:C^α-Arg_{5C}:C^α distance varied considerably during the MD trajectory and that this was mainly influenced by the increased mobility observed in the C-terminal part of the peptide and possibly from the tendency of this part of the sequence to form a β -turn structure.

In order to correlate the findings from the MD simulation about the motions of the peptide's backbone with the experimental X-ray structure of the bound peptide, the quasi harmonic estimated entropy of the backbone atoms has been calculated and compared with the B factor values [58, 59] of the C^α atoms of the peptide. The results are illustrated in Fig. 7. The correlation of entropy of the backbone atoms and B-factors was quite good for the N-terminal part of the peptide but relatively poor in the C-terminal part. Thus, under the light of the current study, the mobility of the C-terminal part of the peptide is relatively increased, especially if we take into consideration the physiological temperature of 310 K that the MD simulation was performed. Moreover, the C-terminal part of the peptide is responsible for the peptide/MHC interactions and the observed plasticity in TCR's structure [29] might influence the peptide's mobility.

Interactions Between the pMHC and TCR and the Plasticity of the TCR's CDR Loops

Most interactions between the pMHC and TCR were observed at the MHC/TCR interface. This is well in accordance with the X-ray structure of the complex. The bound peptide interacted with the TCR only through the hydrophobic side chains of Ala_{6C} and Tyr_{7C} residues. A considerable mobility of the complementarity determining

Fig. 8 Backbone alignment of the MHC X-ray structure (colored black) with representative frames of the MD trajectory (colored magenta). Snapshots were taken at 4, 8, 12, 16, and 20 ns. Peptide is shown in stick representation. X-ray initial structure is colored green, while structures from the MD trajectory are colored cyan. The CDR loops of the TCR are also shown with ribbons, from the X-ray structure and red from the MD trajectory, respectively. For the interpretation of colors in this figure, the reader is referenced to the web version of this article (Color figure online)

regions (CDRs) of the TCR has been observed during the MD trajectory, which is pretty well in line with the observed plasticity of TCR [29]. The mobility of the CDR loops is demonstrated in Fig. 8. The mobility of TCR's CDR loops is not surprising result of this MD study. Conformational mobility of CDR loops have been seen in many pMHC/TCR complexes [60]. The most notable fluctuations observed during the 20 ns MD trajectory are discussed below.

The FLRGRAYGL peptide contributed no hydrogen bond to the TCR (Table 2). Only the Ala_{6C}–Tyr_{7C} part of the peptide sequence was accessible to the TCR binding site. Despite the exposure to CDR loops of the TCR and the availability of five potential sites for hydrogen bonding, such an interaction did not occur. Backbone N and O atoms of the Ala_{6C}–Tyr_{7C} region and the hydroxyl group of the tyrosine's side chain remained hydrated for 70–90% of the trajectory frames, leaving no space for direct peptide/TCR contacts. For the X-ray structure of the complex, it has been reported that there is a hydrogen bond between peptide's Gly_{8C}:O and Tyr_{100E}:O^H from CDR3 β chain. This hydrogen bond was completely abolished during the MD trajectory. Although the TCR's high mobility in CDR regions can be blamed for this, it is interesting to search for possible alternative hydrogen bond donors/acceptors for these two atoms. Thus, it was found that Gly_{8C}'s backbone carbonyl group preferred to form a hydrogen bond with Trp_{147A}:N^H atom from MHC's α chain. Exactly the same interaction has been found in the pMHC complex [61], thus prior to the pMHC/TCR association. On the other hand, Tyr's side chain was found highly hydrated with at least one water molecule (or two for approximately half of the trajectory frames). Gly's carbonyl group was also found hydrated in approximately 45% of the frames. However, a water hydrogen bond was not observed. Most of the water molecules that interacted with Gly's carbonyl group they interacted also with Tyr_{100D}'s side chain, but not at the same time. It was more like a ping-pong interchange of hydrogen bond partners, than a water mediated hydrogen bond interactions.

Tyr_{7C}'s side chain, which pivoted the peptide/TCR interactions [29], was found to form two hydrogen bonds

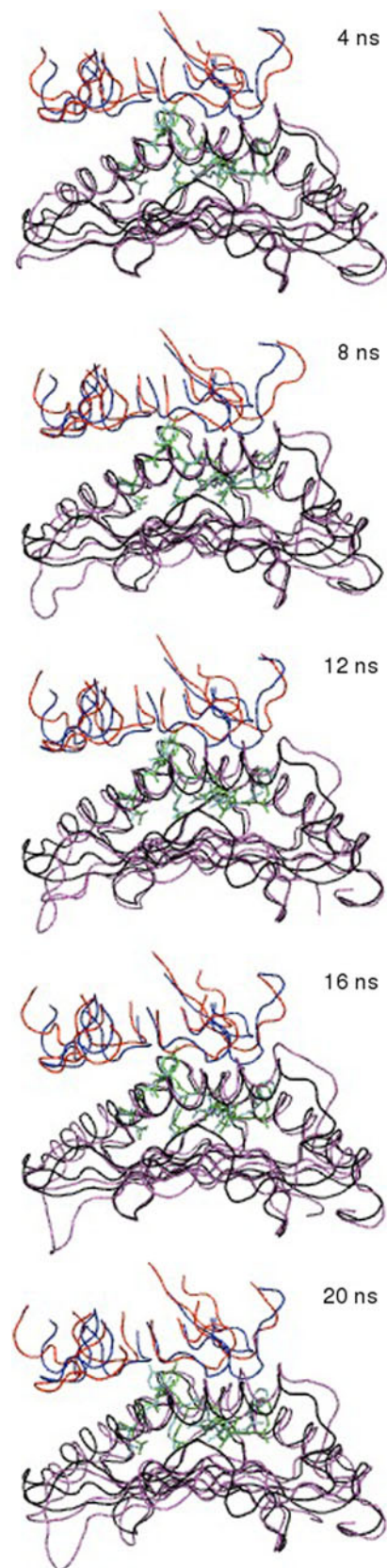


Table 2 Hydrogen bonds between peptide atoms and the MHC molecule

Peptide	MHC	PDB	MD
Phe _{1C} :N	Tyr _{7A} :O ^η	2.92	30.4
Phe _{1C} :O	Tyr _{159A} :O ^η	2.62	97.9
Leu _{2C} :N	Asn _{63A} :O ^{δ1}	3.02	21.7
	Tyr _{99A} :O ^η	3.13	85.3
Arg _{3C} :O	Asn _{70A} :N ^{δ2}	3.02	90.2
Arg _{3C} :N ^ε	Asp _{156A} :O ^{δ1}	4.01	73.7
	Asp _{156A} :O ^{δ2}	3.93	17.0
Arg _{3C} :N ^{η1}	Asn _{114A} :O ^{δ1}	3.60	36.0
	Ser _{97A} :O ^γ	5.65	21.8
	Tyr _{116A} :O ^η	3.53	17.9
Arg _{3C} :N ^{η2}	Asp _{156A} :O ^{δ1}	3.21	56.3
	Asp _{156A} :O ^{δ2}	2.71	80.3
	Asn _{70A} :O ^{δ1}	2.93	99.2
Arg _{5C} :N	Asn _{70A} :O	4.49	33.2
Arg _{5C} :N ^ε	Asp _{74A} :O ^{δ1}	2.76	42.2
	Asp _{9A} :O ^{δ1}	4.30	89.2
Arg _{5C} :N ^{η1}	Asp _{9A} :O ^{δ2}	3.18	0.0
	Asp _{74A} :O ^{δ1}	3.49	15.1
	Asp _{74A} :O ^{δ2}	2.64	87.2
	Asp _{9A} :O ^{δ1}	4.62	25.7
Arg _{5C} :N ^{η2}	Asp _{9A} :O ^{δ2}	3.06	86.5
	Thr _{73A} :O ^{γ1}	2.68	99.5
Arg _{5C} :O	Gln _{98E} :N ^{ε2}	3.06	36.5
Ala _{6C} :O	Lys _{146A} :N ^ζ	3.31	8.2
	Trp _{147A} :N ^{ε1}	3.25	97.2
Leu _{9C} :N	Ser _{77A} :O ^γ	2.69	69.2
Leu _{9C} :O ^{τ1}	Asn _{80A} :N ^{δ2}	3.10	47.6
	Tyr _{123A} :O ^η	6.54	67.0
	Thr _{143A} :O ^{γ1}	4.83	26.4
	Lys _{146A} :N ^ζ	2.66	98.2
Leu _{9C} :O ^{τ1}	Lys _{146A} :N ^ζ	3.43	80.4
	Asn _{80A} :N ^{δ2}	4.55	13.3
	Tyr _{84A} :O ^η	2.89	0.0
	Thr _{143A} :O ^{γ1}	2.96	0.1

The PDB column lists the corresponding distance in the PDB file 1mi5. The MD column lists the percentage of the trajectory frames that satisfied the hydrogen bond criteria, distance donor–acceptor <3.3 Å and angle donor–hydrogen–acceptor >120°

with water molecules for most of the simulation time. In turn, one or two water mediated hydrogen bonds were formed with His_{33D} or His_{48D} side chains. The hydration of the side chains was not an obstacle for the hydrophobic contacts between Tyr_{7C} and Ala_{99D}, Tyr_{100E} side chains from CDR3β of the TCR (Table 3). Indeed, these two hydrophobic residues made significant contacts with the TCR. As it has been reported for the JM22 TCR [62], the Vβ domain makes the most dominant interactions with

Table 3 Hydrophobic side chain interactions between the peptide and MHC or T-cell receptors

MHC	Peptide	PDB	% of MD	Ave. MD
Tyr _{59A}	Phe _{1C}	6.4	53.9	4.0 (0.4)
Ile _{66A}		7.5	43.9	4.1 (0.5)
Trp _{167A}		4.5	32.4	4.5 (0.8)
Tyr _{7A}	Leu _{2C}	5.9	67.1	3.9 (0.3)
Phe _{36A}		6.7	62.8	3.9 (0.3)
Ile _{66A}		4.7	34.6	4.3 (0.5)
Ala _{150A}	Tyr _{7C}	5.2	53.0	4.0 (0.3)
Val _{152A}		4.8	65.8	3.9 (0.4)
Leu _{81A}	Leu _{9C}	6.0	69.7	3.9 (0.4)
Leu _{95A}		7.8	79.0	3.8 (0.3)
Tyr _{116A}		6.6	50.9	4.0 (0.3)
Tyr _{123A}		6.4	45.0	4.0 (0.3)
Trp _{147A}		6.9	93.7	3.6 (0.2)
TCR				
(r)1-1 Leu _{94D}	Ala _{6C}	4.3	75.8	3.8(0.3)
Ala _{99E}		3.9	36.4	4.2(0.4)
Ala _{99E}	Tyr _{7C}	4.0	84.5	3.7(0.3)
Tyr _{100E}		3.9	46.1	4.3(0.8)

The inter-residue distance was measured as the minimum distance between any pair of side chain heavy atoms. The table lists the percentage of the trajectory frames with distance less than 4 Å (% of MD column) and the corresponding distance in the initial X-ray structure (PDB column). The average distance measured from MD trajectory frames (and standard deviation) is listed in the last column (ave. MD)

the MHC. As it is listed in Table 3, the residues Leu_{94E} (CDR3α), Ala_{99E}, and Tyr_{100E} (CDR3β) remained very close to the exposed peptide residues for almost all of the simulation time. The average distance values are very close to those observed in the X-ray structure.

Table 4 lists the hydrogen bonds found between the MHC the TCR molecules. The interactions between Ser_{28D}:O^γ–Arg_{62A}:N^{η2} and Thr_{30D}:O–Gln_{155A}:N^{ε2} were completely lost during the MD trajectory. After inspection of several type side chain interactions, it was found that the formation of a new salt bridge was responsible the interaction disruption between the MHC and CDR1α of TCR. During the MD trajectory, the Arg_{62A}'s side chain broke the hydrogen bond interaction with Ser_{28D}:O^γ and formed a new salt bridged (which was classified as hydrogen bond for 52% of the MD time) with the Glu_{58A} side chain. Both residues lie on the helical part of MHC's structure and their *i, i + 4* proximity is ideal for side chain stabilization in helices [50, 63]. The initial distance in X-ray structure of the pMHC/TCR complex between Arg_{62A}:C^ε and Glu_{62A}:C^γ was 13.9 Å, while the corresponding distance in the X-ray structure of the pMHC complex (PDB code 1m05) was 9.6 Å. Side chain flexibility and charged interactions can accommodate easily such movements of

Table 4 Hydrogen bonds between the MHC and TCR. The PDB column lists the corresponding distance in the PDB file 1mi5

MHC	TCR	PDB	MD
Gln _{65A} :O ^{ε1}	Ser _{99D} :O ^γ	7.19	56.4
Lys _{68A} :N ^ζ	Asp _{56E} :O ^{δ1}	13.55	63.4
	Asp _{56E} :O ^{δ2}	14.17	12.8
Thr _{69A} :O ^{γ1}	Gly _{97D} :O	2.95	3.5
	Thr _{98D} :O	3.15	89.2
Gln _{72A} :O	Gln _{50E} :N ^{ε2}	3.05	0.0
Gln _{72A} :N ^{ε2}	Gln _{98E} :O ^{ε1}	2.67	0.0
Thr _{73A} :O ^{γ1}	Gln _{98E} :N ^{ε2}	3.06	4.8
Arg _{79A} :N ^{η1}	Glu _{52E} :O ^{ε1}	3.93	65.0
	Glu _{52E} :O ^{ε2}	2.86	0.5
Arg _{79A} :N ^{η2}	Asn _{51E} :O ^{δ1}	3.37	57.3
	Glu _{52E} :O ^{ε2}	4.20	61.3
Ala _{150A} :O	Tyr _{31D} :O ^η	4.06	82.9
Arg _{151A} :N ^{η1}	Tyr _{31D} :O ^η	7.47	29.0
Glu _{154A} :O ^{ε1}	Thr _{51D} :O ^{γ1}	4.94	33.6
	Ser _{52D} :O ^γ	3.68	15.1
Glu _{154A} :O ^{ε1}	Arg _{70D} :N ^{η2}	9.99	89.2
Glu _{154A} :O ^{ε2}	Arg _{70D} :N ^{η2}	12.03	83.9

The MD column lists the percentage of the trajectory frames that satisfied the hydrogen bond criteria, distance donor–acceptor <3.3 Å and angle donor–hydrogen–acceptor >120°

approximately 10 Å in residues that lie in $i, i + 4$ positions in α -helices. However, the disruption of the interaction between CDR1 α and the MHC must be noted.

Water Around the Peptide

A considerable number of water molecules made hydrogen bond interactions with the peptide. Table 5 lists the average number of hydrogen bond interactions that involved the peptide and water molecules per residue during the MD trajectory. The peptide, despite being completely surrounded by the MHC and TCR receptors, remained fully hydrated during the MD trajectory. Approximately, 17 water molecules were found in peptide's vicinity. Most polar groups of the peptide made significant hydrogen bonds with the solvent molecules. This is more evident in the C-terminal part of the peptide, in line the observed increased flexibility. The role of water in assisting complex formation between peptide and MHC molecules has been very well addressed in the literature [64]. Most of the water molecules were found around the charged N- and C-terminus of the peptide, as well as the side chain of Tyr₇. Arginine residues at position P3 and P5 contributed only minor interactions with the solvent, as they remained deeply bound in MHC's groove.

Table 5 Average number of hydrogen bonds formed with peptide's donor or acceptor atoms with water molecules during the MD trajectory

Residue	Acceptor	Donor
Phe ₁		2.7 (0.6)
Leu ₂	0.8 (0.4)	
Arg ₃		1.6 (1.0)
Gly ₄	1.5 (0.6)	0.8 (0.4)
Arg ₅		0.2 (0.4)
Ala ₆	1.0 (0.4)	0.9 (0.4)
Tyr ₇	2.1 (0.8)	1.5 (0.6)
Gly ₈	0.4 (0.5)	0.8 (0.5)
Leu ₉	2.7 (1.6)	
Total	8.5 (2.0)	8.7 (1.7)

Hydrogen bonds were evaluated with geometrical criteria (see methods for details). The column acceptor lists the average number of hydrogen bonds where acceptor was a peptide's atom and donor the water's –OH group, while the donor column lists the average number of hydrogen bonds where donor was a peptide's atom and acceptor the water's oxygen atom. Values in parentheses indicate standard deviations

Buried Surface Area

The BSA at the interface of associated biomolecules can be used in order to explore protein's structure and function [65]. Here, the BSA of several parts of the pMHC/TCR complex has been examined. Thus, the complex was split in pMHC–TCR, peptide–MHC, peptide–TCR, and MHC–TCR pairs in order to see the individual contributions in the BSA on the pMHC/TCR association. All frames of the MD trajectory have been extracted and the BSA for each pair has been computed with the NACCESS program. The results of these calculations are shown at Fig. 9. As it can be seen from this illustration, the complex remained stable throughout the 20 ns of the simulation. The stationarity of the BSA lines of each one of the four pairs of interacting species implies that there was no major conformational change during the simulation time. Interestingly, the pMHC/TCR interface was dominated by the MHC/TCR contacts. The BSA of peptide/TCR was approximately only 1/4 of the BSA of the MHC/TCR BSA. This is consistent with the rearrangement of some residues of the MHC molecules, after the TCR binding of the pMHC complex to finely fit the TCR interface [29].

Conclusions

The structures of the pMHC/TCR complexes are characterized by considerable flexibility. As new structures are solved, this becomes more and more evident. Molecular dynamics simulations, based on experimentally determined

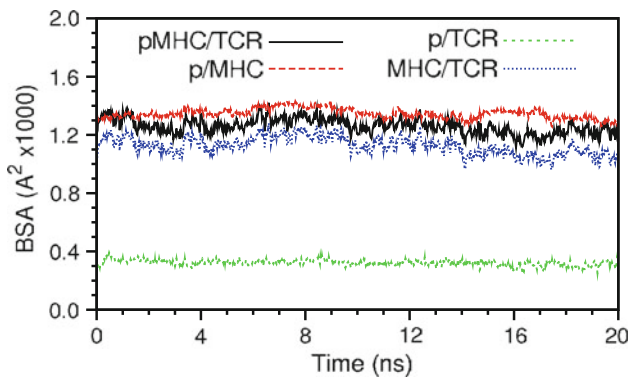


Fig. 9 Time evolution of buried surface is between selected parts of the pMHC/TCR complex. For the interpretation of colors in this figure, the reader is referred to the web version of this article

initial conformations of such complexes can help in investigating the dynamics of the pMHC/TCR assembly. In this study, a state of art molecular dynamics computer simulation of the complex between the HLA-B8 molecule, a peptide that arises from CTL response to *Epstein-Barr virus* and the LC13 T-cell receptor has been utilized in order to elucidate the dynamics of the binding process. The findings are in general in line with the experimentally determined structure. However, considerable new insights have been elucidated.

The peptide's structure is not static. Despite the big similarities in peptide's structure in pMHC and pMHC/TCR complexes (thus before and after the recognition of the pMHC complex by the TCR), the current study suggests a more dynamic view of the peptide. The secondary structure of the peptide can be characterized as open type β -turn in the region Arg_{5C}–Gly_{8C}. This part of the peptide made significant contacts with the TCR. Exposed loops and β -turns are found routinely in protein/protein interfaces. However, this is the first time that this fact is demonstrated in a pMHC/TCR interface. This view is enhanced by the conformational energy landscape analysis of the peptide's structure, which indicated the presence of at least two conformational clusters. This is an interesting finding, because the peptide is completely “stacked” between the MHC's binding groove and the TCR's CDR loops, thus having little space for maneuvers.

The peptide made significant number of hydrogen bonds with the solvent. Approximately, 17 hydrogen bonds were formed between the peptide and the water molecules. Thus, both MHC and TCR receptors “see” a fully hydrated peptide. The solvent does not prevent the recognition, and plays an important role in stabilizing the structure of the complex. Similar observations have been made in the literature for other complexes [66].

Several MHC/TCR contacts showed increased variability. Some interactions found in the X-ray structure

disappeared or existed in a weak mode. Some other emerged through the simulation time, indicating the dynamic view of the pMHC/TCR association. Further work in the future should include entropic analysis of this flexibility in order to quantitatively access this mode of protein/protein association.

Acknowledgments Parallel execution of NAMD was performed at the Research Center for Scientific Simulations (RCSS) of the University of Ioannina. The open source community (Linux, NAMD, GNU, etc.) is gratefully acknowledged for public release of all the necessary computer software needed for this research work.

References

1. Alberts, B., Johnson, A., Lewis, J., Raff, M., Roberts, K., & Walters, P. (Eds.). (2002). *Molecular biology of the cell* (4th ed.). New York: Garland Science.
2. Kaas, Q., & Lefranc, M. P. (2005). T cell receptor/peptide/MHC molecular characterization and standardized pMHC contact sites in IMGT/3D structure-DB. *In Silico Biology*, 5, 505–528.
3. Marrack, P., Scott-Browne, J. P., Dai, S., Gapin, L., & Kappler, J. W. (2008). Evolutionarily conserved amino acids that control TCR-MHC interaction. *Annual Reviews in Immunology*, 26, 171–203.
4. Armstrong, K. M., Insaiddoo, F. K., & Baker, B. M. (2008). Thermodynamics of T-cell receptor-peptide/MHC interactions: progress and opportunities. *Journal of Molecular Recognition*, 21, 275–287.
5. Stone, J. D., Chervin, A. S., & Kranz, D. M. (2009). T-cell receptor binding affinities and kinetics: Impact on T-cell activity and specificity. *Immunology*, 126, 165–176.
6. Savage, P. A., Boniface, J. J., & Davis, M. M. (1999). A kinetic basis for T cell receptor repertoire selection during an immune response. *Immunity*, 10, 485–492.
7. Valitutti, S., & Lanzavecchia, A. (1997). Serial triggering of TCRs: A basis for the sensitivity and specificity of antigen recognition. *Immunology Today*, 18, 299–304.
8. Krogsgaard, M., Prado, N., Adams, E. J., He, X., Chow, D. C., Wilson, D. B., et al. (2003). Evidence that structural rearrangements and/or flexibility during TCR binding can contribute to T cell activation. *Molecular Cell*, 12, 1367–1378.
9. Borbulevych, O. Y., Piepenbrink, K. H., Gloor, B. E., Scott, D. R., Sommese, R. F., Cole, D. K., et al. (2009). T cell receptor cross-reactivity directed by antigen-dependent tuning of peptide-MHC molecular flexibility. *Immunity*, 31, 885–896.
10. Mazza, C., Auphan-Anezin, N., Gregoire, C., Guimezanes, A., Kellenberger, C., Roussel, A., et al. (2007). How much can a T-cell antigen receptor adapt to structurally distinct antigenic peptides? *The EMBO Journal*, 26, 1972–1983.
11. Hansson, T., Oostenbrink, C., & van Gunsteren, W. F. (2002). Molecular dynamics simulations. *Current Opinion in Structural Biology*, 12, 190–196.
12. Karplus, M. (2003). Molecular dynamics of biological macromolecules: A brief history and perspective. *Biopolymers*, 68, 350–358.
13. van Gunsteren, W. F., & Dolenc, J. (2008). Biomolecular simulation: historical picture and future perspectives. *Biochemical Society Transactions*, 36, 11–15.
14. Aksimentiev, A., Brunner, R., Cohen, J., Comer, J., Cruz-Chu, E., Hardy, D., et al. (2008). Computer modeling in biotechnology: A partner in development. *Methods in Molecular Biology*, 474, 181–234.

15. Mobley, D. L., & Dill, K. A. (2009). Binding of small-molecule ligands to proteins: “what you see” is not always “what you get”. *Structure*, *17*, 489–499.
16. van Gunsteren, W. F., Dolenc, J., & Mark, A. E. (2008). Molecular simulation as an aid to experimentalists. *Current Opinion in Structural Biology*, *18*, 149–153.
17. Mallik, B., & Morikis, D. (2006). Applications of Molecular Dynamics Simulations in immunology: A useful computational method in aiding vaccine design. *Current Proteomics*, *3*, 259–270.
18. Michielin, O., & Karplus, M. (2002). Binding free energy differences in a TCR-peptide-MHC complex induced by a peptide mutation: a simulation analysis. *Journal of Molecular Biology*, *324*, 547–569.
19. Morikis, D., & Lambris, J. D. (2004). Physical methods for structure, dynamics and binding in immunological research. *Trends in Immunology*, *25*, 700–707.
20. Stavrakoudis, A. (2009). A disulfide linked model of the complement protein C8 γ complexed with C8 α indel peptide. *Journal of Molecular Modeling*, *15*, 165–171.
21. Stavrakoudis, A. (2010). Conformational flexibility in designing peptides for immunology: The molecular dynamics approach. *Current Computer-Aided Drug Design*, *6*, 207–222.
22. Wan, S., Flower, D. R., & Coveney, P. V. (2008). Toward an atomistic understanding of the immune synapse: large-scale molecular dynamics simulation of a membrane-embedded TCR-pMHC-CD4 complex. *Molecular Immunology*, *45*, 1221–1230.
23. Flower, D. R., Phadwal, K., Macdonald, I. K., Coveney, P., Davies, M. N., & Wan, S. (2010). T-cell epitope prediction and immune complex simulation using molecular dynamics: State of the art and persisting challenges. *Immunome Research*, *6*(Suppl 2), S4. doi:10.1186/1745-7580-6-S2-S4.
24. Sadiq, S. K., Mazzeo, M. D., Zasada, S. J., Manos, S., Stoica, I., Gale, C. V., et al. (2008). Patient-specific simulation as a basis for clinical decision-making. *Philosophical Transactions of the Royal Society A*, *366*, 3199–3219.
25. Cuendet, M. A., & Michielin, O. (2008). Protein-protein interaction investigated by steered molecular dynamics: The TCR-pMHC complex. *Biophysical Journal*, *95*, 3575–3590.
26. Wan, S., Coveney, P. V., & Flower, D. R. (2005). Peptide recognition by the T cell receptor: Comparison of binding free energies from thermodynamic integration, Poisson-Boltzmann and linear interaction energy approximations. *Philosophical Transactions of the Royal Society A*, *363*, 2037–2053.
27. Zoete, V., & Michielin, O. (2007). comparison between computational alanine scanning and per-residue binding free energy decomposition for protein-protein association using MM-GBSA: Application to the TCR-p-MHC complex. *Proteins: Structure, Function, and Bioinformatics*, *67*, 1026–1047.
28. Zoete, V., Irving, M. B., & Michielin, O. (2009). MM-GBSA binding free energy decomposition and T cell receptor engineering. *Journal of Molecular Recognition*, *23*, 142–152.
29. Kjer-Nielsen, L., Clements, C. S., Purcell, A. W., Brooks, A. G., Whisstock, J. C., Burrows, S. R., et al. (2003). A structural basis for the selection of dominant alphabeta T cell receptors in antiviral immunity. *Immunity*, *18*, 53–64.
30. Koch, O., & Klebe, G. (2009). Turns revisited: A uniform and comprehensive classification of normal, open, and reverse turn families minimizing unassigned random chain portions. *Proteins: Structure, Function, and Bioinformatics*, *74*, 353–357.
31. Berman, H. M., Battistuz, T., Bhat, T. N., Bluhm, W. F., Bourne, P. E., Burkhardt, K., et al. (2002). The protein data bank. *Acta Crystallographica Section D*, *58*, 899–907.
32. Humphrey, W., Dalke, A., & Schulten, K. (1996). VMD: Visual molecular dynamics. *Journal of Molecular Graphics*, *14*, 33–38.
33. Feller, S. E., & MacKerell, A. D., Jr. (2000). An improved empirical potential energy function for molecular simulations of phospholipids. *The Journal of Physical Chemistry B*, *104*, 7510–7515.
34. Word, J. M., Lovell, S. C., Richardson, J. S., & Richardson, D. C. (1999). Asparagine and glutamine: using hydrogen atom contacts in the choice of side-chain amide orientation. *Journal of Molecular Biology*, *285*, 1735–1747.
35. Mark, P., & Nilsson, L. (2001). Structure and dynamics of the TIP3P, SPC, and SPC/E water models at 298 K. *The Journal of Physical Chemistry A*, *105*, 9954–9960.
36. Weber, W., Hunenberger, P. H., & McCammon, J. A. (2000). Molecular dynamics simulations of a polyalanine octapeptide under Ewald boundary conditions: influence of artificial periodicity on peptide conformation. *The Journal of Physical Chemistry B*, *104*, 3668–3675.
37. Darden, T., York, D., & Pedersen, L. (1993). Particle mesh Ewald: An Mlog(N) method for Ewald sums in large systems. *Journal of Chemical Physics*, *98*, 10089–11092.
38. Ryckaert, J. P., Ciccotti, G., & Berendsen, H. J. C. (1977). Numerical integration of the Cartesian equations of motion of a system with constraints: Molecular dynamics of *n*-alkanes. *Journal of Computational Physics*, *23*, 327–341.
39. Feller, S. E., Zhang, Y., Pastor, R. W., & Brooks, B. R. (1995). Constant pressure molecular dynamics simulation: The Langevin piston method. *The Journal of Physical Chemistry B*, *103*, 4613–4621.
40. Tsoulos, I. G., & Stavrakoudis, A. (2011). Eucb: A C++ program for molecular dynamics trajectory analysis. *Computer Physics Communications*, *182*, 834–841.
41. Döker, R., Maurer, T., Kremer, W., Neidig, K., & Kalbitzer, H. R. (1999). Determination of mean and standard deviation of dihedral angles. *Biochemical and Biophysical Research Communications*, *257*, 348–350.
42. Yamartino, R. J. (1984). A comparison of several “single-pass” estimators of the standard deviation of wind direction. *Journal of Climate and Applied Meteorology*, *23*, 1362–1366.
43. Hutchinson, E. G., & Thornton, J. M. (1994). A revised set of potentials for beta-turn formation in proteins. *Protein Science*, *3*, 2207–22016.
44. Wilmot, C. M., & Thornton, J. M. (1988). Analysis and prediction of the different types of β -turn in proteins. *Journal of Molecular Biology*, *203*, 221–232.
45. Glykos, N. M. (2006). Carma: A molecular dynamics analysis program. *Journal of Computational Chemistry*, *27*, 1765–1768.
46. Hubbard, S. (1996). Naccess V2.1.1—atomic solvent accessible area calculations. <http://www.bioinf.manchester.ac.uk/naccess/>.
47. Schlitter, J. (1993). Estimation of absolute and relative entropies of macromolecules using the covariance matrix. *Chemical Physics Letters*, *215*, 617–621.
48. Andricioaei, I., & Karplus, M. (2001). On the calculation of entropy from covariance matrices of the atomic fluctuations. *The Journal of Chemical Physics*, *115*, 6289.
49. Buck, M., Bouguet-Bonnet, S., Pastor, R. W., & MacKerell, A. D., Jr. (2006). Importance of the CMAP correction to the CHARMM22 protein force field: Dynamics of hen lysozyme. *Biophysical Journal*, *90*, 36–38.
50. Stavrakoudis, A. (2008). Molecular dynamics simulations of an apolipoprotein derived peptide. *Chemical Physics Letters*, *461*, 294–299.
51. Mu, Y., Nguyen, P. H., & Stock, G. (2005). Energy landscape of a small peptide revealed by dihedral angle principal component analysis. *Proteins: Structure, Function, and Bioinformatics*, *58*, 45–52.
52. Fadoulglou, V. E., Stavrakoudis, A., Bouriotis, V., Kokkinidis, M., & Glykos, N. M. (2009). Molecular Dynamics simulations of

- BcZBP, a deacetylase from bacillus cereus: active site loops determine substrate accessibility and specificity. *The Journal of Chemical Theory and Computation*, 5, 3299–3311.
53. Hoare, H. L., Sullivan, L. C., Clements, C. S., Ely, L. K., Beddoe, T., Henderson, K., et al. (2008). Subtle changes in peptide conformation profoundly affect recognition of the non-classical MHC class I molecule HLA-E by the CD94–NKG2 natural killer cell receptors. *Journal of Molecular Biology*, 377, 1297–1303.
 54. Frishman, D., & Argos, P. (1995). Knowledge-based protein secondary structure assignment. *Proteins: Structure, Function and Genetics*, 23, 566–579.
 55. Stewart-Jones, G. B., Gillespie, G., Overton, I. M., Kaul, R., Roche, P., McMichael, A. J., et al. (2005). Structures of three HIV-1 HLA-B*5703-peptide complexes and identification of related HLAs potentially associated with long-term nonprogression. *Journal of Immunology*, 175, 2459–2468.
 56. Archbold, J. K., Macdonald, W. A., Gras, S., Ely, L. K., Miles, J. J., Bell, M. J., et al. (2009). Natural micropolymorphism in human leukocyte antigens provides a basis for genetic control of antigen recognition. *Journal of Experimental Medicine*, 206, 209–219.
 57. Tatsis, V. A., Tsoulos, I. G., & Stavrakoudis, A. (2009). Molecular dynamics simulations of the TSSPSAD Peptide Antigen in free and bound with CAMPATH-1H Fab antibody states: the importance of the β -turn conformation. *International Journal of Peptide Research and Therapeutics*, 15, 1–9.
 58. Glykos, N. (2007). On the application of molecular-dynamics simulations to validate thermal parameters and to optimize TLS-group selection for macromolecular refinement. *Acta Crystallographica Section D*, D63, 705–713.
 59. Meirovitch, H., & Hendrickson, T. F. (1997). Backbone entropy of loops as a measure of their flexibility: application to a ras protein simulated by molecular dynamics. *Proteins: Structure, Function, and Bioinformatics*, 29, 127–140.
 60. Armstrong, K. M., Piepenbrink, K. H., & Baker, B. M. (2008). Conformational changes and flexibility in T-cell receptor recognition of peptide-MHC complexes. *Biochemical Journal*, 415, 183–196.
 61. Kjer-Nielsen, L., Clements, C. S., Brooks, A. G., Purcell, A. W., Fontes, M., McCluskey, J., et al. (2002). The structure of HLA-B8 complexed to an immunodominant viral determinant: Peptide-induced conformational changes and a mode of MHC class I dimerization. *The Journal of Immunology*, 169, 5153–5160.
 62. Ishizuka, J., Stewart-Jones, G. B. E., van der Merwe, A., Bell, J. I., McMichael, A. J., & Jones, E. Y. (2008). The structural dynamics and energetics of an immunodominant T cell receptor are programmed by its V β domain. *Immunity*, 28, 171–182.
 63. Marqusee, S., & Baldwin, R. L. (1987). Helix stabilization by Glu-...Lys + salt bridges in short peptides of de novo design. *Proceedings of the National Academy of Sciences of the United States of America*, 84, 8898–8902.
 64. Petrone, P. M., & Garcia, A. E. (2004). MHC-peptide binding is assisted by bound water molecules. *Journal of Molecular Biology*, 338, 419–435.
 65. Rashin, A. (1984). Buried surface area conformational entropy, and protein stability. *Biopolymers*, 23, 1605–1620.
 66. Wong, S., Amaro, R. E., & McCammon, J. A. (2009). MM-PBSA captures key role of intercalating water molecules at a protein-protein interface. *The Journal of Chemical Theory and Computation*, 5, 422–429.